PAPER

Study of the structure of a multicomponent salt melt using molecular dynamics modeling

IOP Publishing Journal of Physics: Condensed Matter
J. Phys.: Condens. Matter **33** (2021) 495103 (10pp) https://doi.org/10.1088/1361-648X/ac26fa

Study of the structure of a multicomponent salt melt using molecular dynamics modeling

Alexander Y Galashev[1,2,*]

Institute of High-Temperature Electrochemistry, Ural Branch, Russian Academy of Sciences, Yekaterinburg 620990, Russia
Ural Federal University named after the first President of Russia B.N. Yeltsin, Yekaterinburg 620002, Russia

E-mail: galashev@ihte.uran.ru

Received 17 June 2021, revised 8 September 2021
Accepted for publication 15 September 2021
Published 4 October 2021

Abstract

The composition of the electrolyte is critical in the electrodeposition of high-purity silicon. In this work, molecular dynamics modeling of the preparation of liquid salt melt KF–KCl–KI and a detailed study of its structure based on the method of statistical geometry have been performed. Partial radial distribution functions reflect the size of the ions under consideration and the averaged structure of the generated ionic subsystems. Halogen subsystems have domed angular distributions of nearest geometric neighbors, a wide range of face types of combined polyhedra, and fifth order rotational symmetry. The shape of the distribution of distances to the nearest neighbors of a given type depends on the amount of these ions in the melt. Small-scale thermal fluctuations in the halogen subsystems are predominantly represented by small triangular faces in combined polyhedra. The electrodeposition of silicon was carried out in a homogeneous salt melt, in which each halogen ion had from one to three close contacts with halogen ions of any other type. The simulations performed provide a fundamental understanding of the structure of the electrolyte molten salts used to produce solar silicon.

Keywords: melt, molecular dynamics, structure, Voronoi polyhedron

S Supplementary material for this article is available online

(Some figures may appear in colour only in the online journal)

1. Introduction

Among the renewable energy sources, which are receiving more and more attention, solar cells occupy the leading place [1, 2]. Silicon solar cells occupy a dominant position in their production. The competitiveness of such devices is determined by the efficiency of energy conversion and the reduction in the cost of modules. This task cannot be solved only by introducing an innovative cell structure. Reducing the cost of modules can be achieved through the use of inexpensive advanced technologies for the production of high-purity silicon.

The production of silicon wafers is the most costly process, which involves complex processing, intense energy consumption and high temperature for silicon crystallization [3]. The approach of obtaining silicon at low temperatures in liquid/molten salts turned out to be promising [4, 5]. However, this has its own problem related to the control of impurities. The optimal electrolyte composition proved to be the cornerstone in obtaining the photoelectric effect for the deposited silicon film.

* Author to whom any correspondence should be addressed.

Water-based electrolytes are not suitable for silicon electrodeposition [6]. An electrolyte for this purpose can be a high-temperature molten salt [7, 8], or an organic electrolyte [9, 10]. Volatile solvents in the electrolyte can have high vapor pressure and are highly flammable, which is unsafe. Ionic liquids with low volatility at room temperature are generally expensive. An important requirement is that the silicon deposit be free of electrolyte decomposition products.

It has been shown experimentally that the KF–KCl–KI melt, supplemented with 0.075–0.5 mol% K_2SiF_6 content, is not too aggressive and ensures stable deposition of a silicon film without leaving unfavorable precipitation in it [11]. The aggressiveness of this electrolyte is reduced by its high KI (75 mol%) content. Thin silicon films were obtained by electrodeposition under galvanostatic conditions at 998 K. Considered a salt melt had a melting point lower than 973 K, because the final melting of the system the KF–KCl (2:1) –75 mol% KI melt containing 0.075 or 0.5 mol% K_2SiF_6 was carried out precisely at this temperature [11]. According to the thermal analysis data, the melting point of the investigated salt melt should be 858 K [12]. The melting temperature of the melt model, established in [13] from the dramatic break in the temperature dependence of the potential (and total) energy of the considered salt melt, was 847 K. The authenticity of this value is confirmed by a detailed analysis of the melt structure and calculated values of the diffusion coefficients.

The composition of the salt electrolyte is of great importance for obtaining perfect, highly pure silicon films. The presence of associates in the molten salt can adversely affect the uniformity of silicon deposition during electrolysis. Experimental study of obtaining the optimal composition of the KF–KCL–KI electrolyte is difficult. Even thermodynamic analysis requires expensive experimental research methods. There are significant difficulties in working in molten salt containing fluorides. The ionic structure of such a melt is influenced by temperature, strong volatility; fused fluorine salt makes it easy to change its composition.

The molecular dynamics method is an effective and cheaper method for studying the structure of salt melts in comparison with measurements of Raman spectroscopy and nuclear magnetic resonance. An important point when using this method is finding adequate interatomic interaction potentials.

The aim of this work is to develop an inexpensive method for studying the detailed structure of a four-component salt melt, which makes it possible to determine its optimal composition for the production of solar silicon.

1.1. Computational methods

Initially, a numerical model that establishes the potentials from the characteristics of the solid phase of alkali metal halides using a combination of Coulomb terms and short-range repulsive terms was developed by Born, Mayer and Huggins in [14–17]. Tosi and Fumi refined the repulsive part of this potential, including the dipole–quadrupole van der Waals term, that imitated the polarization distortion of the electron cloud [18]. This model satisfactorily predicts the densities and lattice energies of alkali halides, but does not adequately describe the dynamic characteristics of ionic crystals. In addition, the model predicts the same form of the like pair distribution functions, which contradicts the experimental data [19]. It is noted in [20] that the model proposed in [18] is better suited for describing alkali metal halides containing K^+, Cl^-, Na^+, Br^-, and Li^+. At the same time, this model reflects much worse the properties of such systems containing Rb^+ or F^- ions. In another popular model of alkali halides, ion–ion interactions are presented in the Lennard-Jones (LJ) form [21, 22]. To a greater extent, this model has found application in the study of aqueous solutions of alkali metal halides. The models from [21, 22] are less physical, since they do not contain an explanation on the representation of polarization effects. In this work, we use the Born–Mayer–Huggins–Tosi–Fumi (BMHFT) rigid-ion (RI) interionic potential for the molten salts [23] with parameter β changed with respect to the corresponding parameter of the Tosi–Fumi model [18]. This made it possible to correct the location of the first peak of the cation–anion pair correlation functions in molten ternary chlorides [24]. The BMHFT potential reproduces the properties of molten salts LiCl, NaCl and KCl well [24].

The formula representing BMHFT potential is

$$\Phi = Z_i Z_j \frac{e^2}{4\pi\varepsilon_0\varepsilon r} + B_{ij}\exp\left[-\frac{r-\sigma_{ij}}{\beta_{ij}}\right] - \\ - \frac{C_{ij}}{r^6} - \frac{D_{ij}}{r^8} \quad (1)$$

where i and j can represent positive or negative ion, Zi and Zj are ± 1, in the case when the system is completely ionic and dipole–dipole and dipole–quadrupole terms are included; ε_0 and ε are the permittivity of the free space and the studied environment, respectively. The parameters of the BMHFT potential for molten salt KF–KCl–KI, determined in [25–28], are presented in table 1.

The presence of an exponent in the BMHFT potential looks the most physical, since the charge distribution around the ion exponentially decays at a considerable distance from it. Unsurprisingly, the energy calculated using this potential agrees very well with the Hartree–Fock energy. It is known that, in contrast to the systems of noble gases, one set of potentials cannot correctly describe the properties of alkali metal halides simultaneously for the solid, liquid, and gaseous phases [29]. The use of more realistic models that directly take into account ion polarization is not always justified. A more careful consideration of the ion polarization creates significant problems associated with a useless extra cost of the calculation without noticeable benefit of accuracy [30]. However, in the case of simulating aqueous solutions, neglecting polarization leads to incorrect results.

The correct representation of short-range interactions in the study of the ionic system is important, despite the fact that these interactions usually make a small contribution (up to several percent) to the cohesion energy. A fairly simple check of the correctness of the description of short-range interactions can be the achievement of the stability of the crystal lattice inherent in a given ionic system, when the value of the nearest interatomic distance is equal to the experimentally established equilibrium value. This cannot be obtained, for example, using

Table 1. Parameters of the BMHFT potential describing interactions in the KF–KCl–KI salt melt.

	B_{ij} (eV)	β_{ij} (Å)	σ_{ij} (Å)	Cij (eV^{x}Å^{6})	D_{ij} (eV^{x}Å^{8})	Ref.
K–K	0.2641	0.3003	2.926	15.19	−15.0	[15]
K–Cl	0.2113	0.3003	3.048	30.0	−6.438	
Cl–Cl	0.1584	0.3003	3.170	11.576	−13.69	
K–I	0.21098	0.355	3.37	12.135	−15.68	[16]
I–I	0.1592	0.355	3.814	11.5756	−13.691	
K–F	0.2113	0.338	3.1965	12.1358	−13.0689	[17]
F–F	0.1582	0.338	3.143	11.5756	−13.6911	
F–Cl	0.1583	0.3179	3.1565	11.5756	−13.6911	[18]
F–I	0.1587	0.3471	3.4785	11.5756	−13.6911	
Cl–I	0.1588	0.3279	3.492	11.5756	−13.6911	

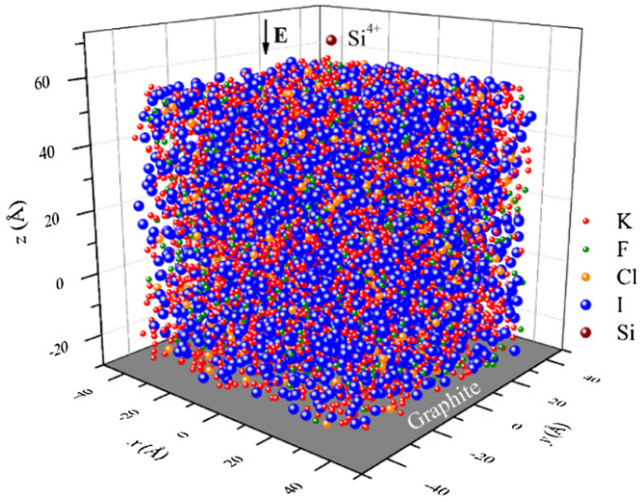

Figure 1. Configuration of the KF–KCl–KI salt melt obtained during the electrodeposition of Si^{4+} ions on a graphite substrate at a temperature of 1000 K and an electric field strength of 10^4 V m^{-1} at the 20 ns time moment.

the Born–Mayer rigid ion potential [30]. A study of the melting temperatures of alkali halide crystals by visual observation showed that the steepness of the repulsive branch of the potential has a significant effect on melting [30]. In particular, the presence of ions with hard core stimulates the retention of the crystal structure.

The studied salt melt had the following composition: KF-19.2 mol%, KCl-9.6 mol%, and KI-71.2 mol%. In this case, the number of K^+ ions was 4496, the number of F^-, Cl^- and I^- ions was 864, 432, and 3200, respectively. This composition of the salt melt is close to the composition of the melt used in a real experiment for silicon electrodeposition.

The system configuration at a time of 20 ns is shown in figure 1. As can be seen from figure 1, in the model of the salt melt KF–KCl–KI, a high mixing of ions is achieved. However, it can be seen that, in addition to the different-grade neighborhoods, small groups of single-grade ions can also be found in the melt, especially the K^+ and I^- ions, the number of which prevails.

The production of mixtures with desired properties may involve the fulfillment of certain requirements or mixing rules. Mixing rules are sometimes used to predict the refractive indices of liquid mixtures, but most often they are needed to impart specific properties to polymers. Data on viscosity and shear rate are usually required to describe the rheological behavior of a viscous system [31]. The mixing rules allow you to analytically determine the final viscosity of a plasticmaterial without resorting to expensive testing. However, for molten salt KF–KCl–KI, there is no need to introduce any rules, because this system is characterized by a rather low dynamic viscosity, which at 1000 K is 1–5 orders of magnitude lower than the extrusion temperature of polymers (∼473 K) and only 2–4 times higher than the corresponding characteristic of water at 293 K. Therefore, in this work, the salt melt was prepared by direct melting of the crystalline components that form the modeled system.

The melt was prepared in several stages by melting the initial components KF, KCl, and KI. At the first stage, the original solid components were placed in a rectangular box. At all stages of the simulation, a constant time step of 1 fs was used to integrate the equations. First, using an NVT ensemble, the system was heated to a temperature of 300 K for 0.1 ns. Then, the system was heated stepwise from 300 K to 1700 K in 28 temperature steps with a step of 50 K. In this case, the execution time of each temperature step was 0.1 ns. The next stage of calculations was carried out in the NPT ensemble. At this stage, the simulated melt reached the required density of 2.12 g cm^{-3} for 1 ns and in further calculations, this density value remains unchanged. The experimentally obtained KF–KCL-75 mol% KI melt at 1000 K has a density of 2.27 g cm^{-3} [32], which is 6.6% higher than that obtained in the present model. Then the system was cooled to a temperature of 1000 K in 0.5 ns.

Molecular dynamics modeling of liquid alkali halloid compounds in the NPT ensemble gives lower melt densities than the corresponding experimental values. So, using a similar form of the interaction potential for pure melts LiCl, NaCl and KCl, densities lower than the experimental ones by 5.3%, 6.3% and 9.0%, respectively, were obtained [33]. The low value of the melt density is due not only to the pair interaction potential used, but also to the accuracy of determining the pressure in a sufficiently small system produced by the NPT ensemble. Even in the *ab initio* molecular dynamics study of molten salts in an NPT ensemble, small errors in energy calculations lead to a significant decrease in the density of the system. It is considered that the system is in an equilibrium state if, over 10

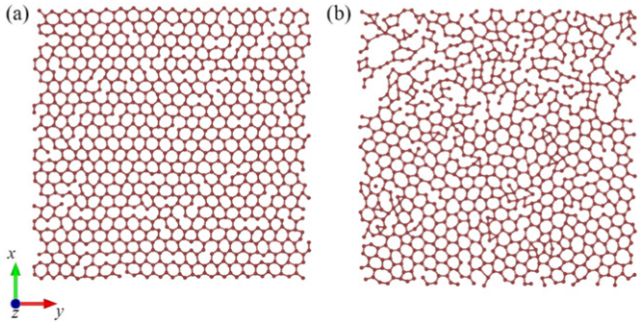

Figure 2. *xy*-projections of two-dimensional silicon at a temperature of $T = 1000$ K, located on a graphite substrate; (a) single-layer silicene (b) deposited silicon film; calculations were performed by MD simulation; the positions of Si atoms in both configurations are averaged over a time interval of 1 ns. The deposited film contains a small number of Si atoms belonging to the second layer.

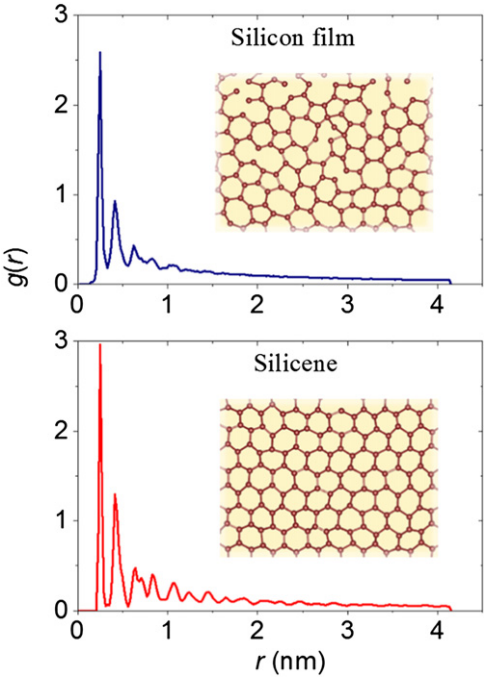

Figure 3. Radial distribution functions obtained for a silicon film deposited on graphite and for silicene lying on graphite at $T = 1000$ K. The insets show fragments of objects corresponding to these functions.

000 time steps ($\Delta t = 0.5$ fs), the energy is conserved within 2% [34]. Note that the duration of our resulting calculation exceeds the specified time interval by 4000 times.

The final configuration of the system obtained in this calculation served as the initial configuration for the main calculation with a duration of 20 ns (20 million time steps), during which the structural characteristics of the melt were determined. At all stages of obtaining an equilibrium salt melt, the periodic boundary conditions (PBC) acted in three mutually perpendicular directions. However, during the electrodeposition of silicon, PBC was carried out only in the 0x and 0y directions, while a constant electric field of 10^4 V m^{-1} acted at the 0z direction.

The electrodeposition of silicon in the model used was carried out by passing Si^{4+} ions through the melt, which were alternately (every 30 ps) launched from random points near the melt surface and moved downward under the action of an applied electric field. Note that the time required for the ion to take its place after reaching the substrate has been usually from 1 to 10 ps. Graphite was used as a substrate for Si deposition. The interaction of atoms in the substrate was described by the Tersoff potential [35]. Interaction of Si^{4+} ion in molten salt was described by the LJ potential with the Coulomb term and the interaction between silicon and melt components as well as the interaction of silicon or salt melt with a graphite substrate were represented by the LJ potential [13]. To determine the parameters of the L-J potential of the Si-halogen and C-halogen, the Berthelot–Lorentz rule was used.

A detailed structural analysis is carried out both on the basis of calculating the partial functions of the radial distribution, and using the construction of combined analogs of Voronoi polyhedra (VP) [36–39]. The combined polyhedron was built around an ion of type i, and ions of another type j served as its nearest geometric neighbors. When constructing the angular distributions of the nearest geometric neighbors (θ distributions), the angles θ with a vertex at the center of the VP are considered, the sides of which pass through the centers of the neighbors that give the faces of the VP. Thus, the angular distribution reflects the probabilities of observing certain values of the angles θ. The distribution of the VP by the number of faces (n distribution) is a topological characteristic showing the probabilities of detecting a certain number of nearest geometric neighbors around the selected ions. The distribution of the VP faces by the number of sides (m distribution) characterizes the probabilities of detecting cyclic formations created certain ions, which can be observed from the VP center in the directions of the nearest geometric neighbors. Combined polyhedra were constructed through every 10 000 time steps for each ion of the ith type. Thus, among halogen ions, the minimum number of polyhedra (0.864 million) was constructed for Cl^- ions, and the maximum (6.4 million)-for I^- ions. The obtained statistical distributions of the geometric elements of the combined polyhedrons characterize the structure of the molten salt during the observation time of the system 20 ns. The angular distributions of the nearest geometrical neighbors constructed using such polyhedra have a domed shape. This form of angular distributions is characteristic of a multicomponent liquid with different sizes of atoms of each component [40]. The partial functions of the radial distribution of the salt melt were determined over the same time interval (20 ns), but they were calculated at each time step. The radial distribution function (RDF) of silicon was also calculated at each time step, but over a shorter time interval (10 000 time steps).

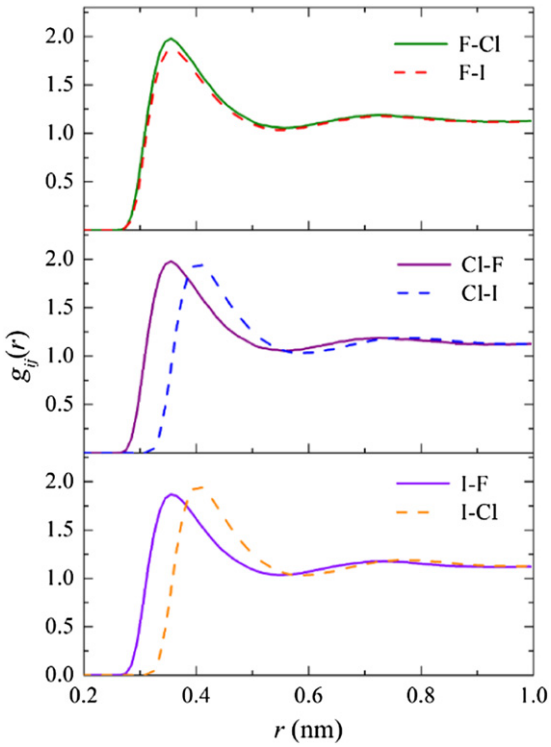

Figure 4. Partial functions of the radial distribution of systems formed by halogens of different types in the salt melt KF–KCl–KI at a temperature of 1000 K; the types of functions $g_{ij}(r)$ are indicated in the margins of the figures.

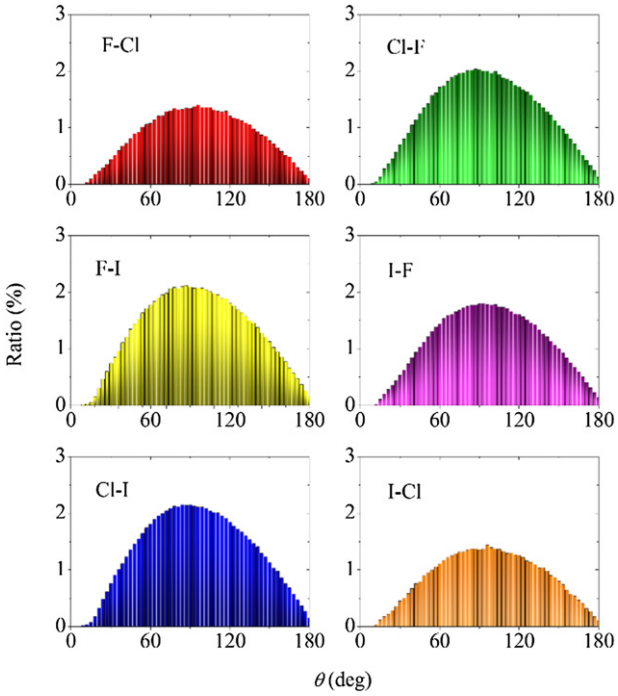

Figure 5. The ratio between the different angles present in the angular distributions of the nearest geometrical neighbors for halogens of different types: the first chemical element corresponds to the ion located at the vertex of the angle θ, and the second to the ions forming the sides of this angle in the molten KF–KCl–KI salt at a temperature of 1000 K.

2. Results and discussion

Since the deposition of silicon from a melt on graphite formed a two-dimensional distorted hexagonal structure, it is of interest to compare this structure with the structure of a single-layer silicene under approximately the same conditions. The *xy*-projections of initially perfect silicene and the silicon film obtained by MD simulation of deposition from the melt are presented in figure 2.

The program we created to determine the bonds in the model recorded only stable bonds, the length of which changed by less than the value of $h/2$ (where $h = 0.044$ nm is the low buckling in freestanding silicene) in a time interval of 1 ps. The unstable bonds, mainly located in the upper part of figure 2(b), are not shown here. The silicene in figure 2(a) is represented by 1008 Si atoms, and the silicon film in figure 2(b) is formed by 982 atoms. Several of the deposited Si atoms in figure 2(b) are above the first silicon layer. After the deposition of the silicon film was completed, the RDF was calculated for the Si film lying on graphite in the absence of a melt. The calculations were performed at a temperature of 1000 K, and their duration was 1 ns. Similar calculations were performed for a single-layer silicene lying on graphite. The calculated radial distribution functions together with the corresponding fragments of the structure of the compared objects are shown in figure 3. The obtained RDFs for the silicon film and silicene are in many respects similar. However, the peaks in RDF for silicene, are more pronounced, emphasizing the higher ordering of this structure.

In this work, the main attention is paid to the study of the structure of the salt melt used to obtain a high-purity silicon film. Partial radial distribution functions are reversible upon permutation of the symbols that describe them, for example, the function $g(r)_{\mathrm{F-Cl}}$ is identical to the function $g(r)_{\mathrm{Cl-F}}$. In figure 4, we present the partial functions $g(r)_{ij}$ for each pair of halogens present in the molten salt. With a relatively small difference in the radii of the Cl^- ($R_{\mathrm{Cl-}} = 0.181$ nm) and I^- ($R_{\mathrm{I-}} = 0.22$ nm) ions, the partial functions $g(r)_{\mathrm{F-Cl}}$ and $g(r)_{\mathrm{F-I}}$ turn out to be quite close with the absence of a shift as the first, and the second peak. However, the difference in the radii of the Cl^- and F^- ions ($R_{\mathrm{F-}} = 0.133$ nm) leads to a shift of these peaks for the $g(r)_{\mathrm{Cl-I}}$ function to the right relative to the corresponding peaks of the $g(r)_{\mathrm{Cl-F}}$ function. The difference in the radii of the F^- and Cl^- ions produces approximately the same effect, so that the function $g(r)_{\mathrm{I-Cl}}$ is shifted to the right relative to the function $g(r)_{\mathrm{I-F}}$.

The angular distributions obtained for halogens of different types of molten salt mixtures are shown in figure 5. The maxima of the distributions presented in figure 5 are located in the range of angles 84°–96°. Moreover, the smallest value of the location of the extremum corresponds to the ionic composition of Cl–I (84°), and the largest—to I–Cl and F–Cl (96° for both).

The distributions of combined polyhedra by the number of faces are not symmetric with respect to the permutation of symbols of chemical elements in their designation. For example, the *n* distribution corresponding to the F–Cl designation is markedly asymmetric, while the corresponding

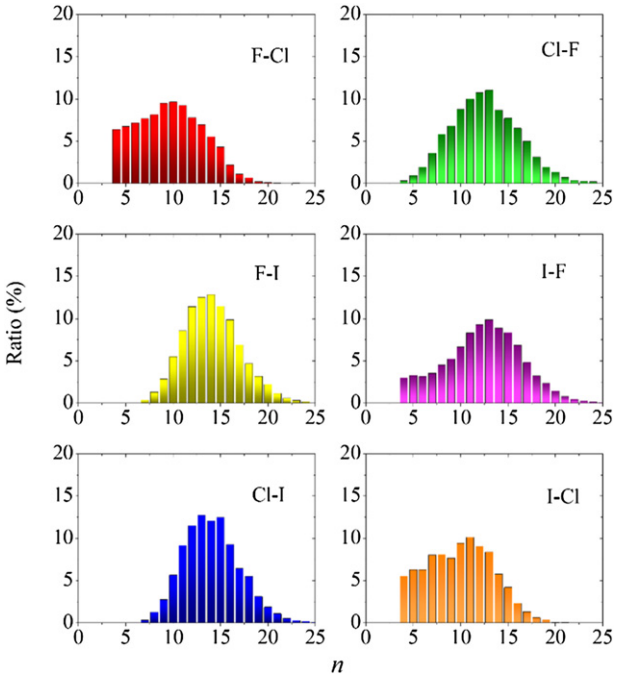

Figure 6. The ratio between the numbers of different faces in combined polyhedra plotted for halogens in the KF–KCl–KI salt melt at 1000 K; the first symbol in the field of each figure refers to the ion located in the center of the polyhedron, and the second characterizes the ions that give the faces of this polyhedron.

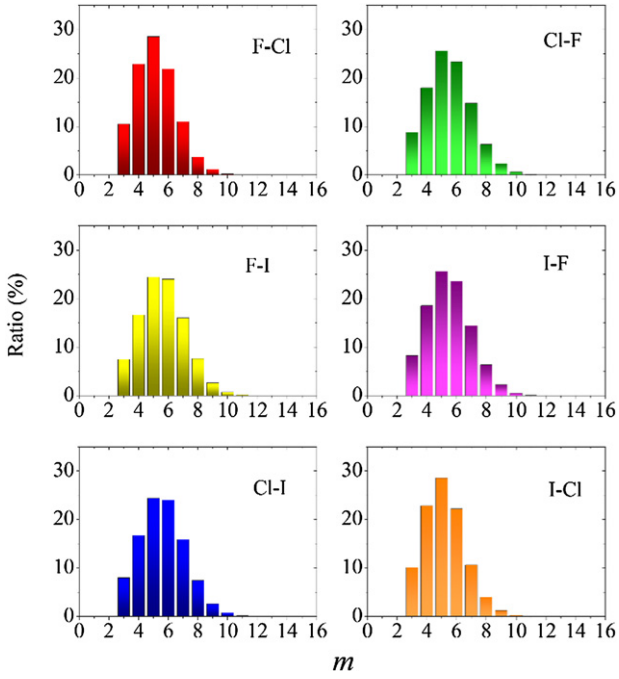

Figure 7. The ratio between the numbers of possible sides in faces for combined polyhedrons characterizing the KF–KCl–KI salt melt at a temperature of 1000 K; the symbols of chemical elements in the field of each figure have the same meaning as the symbols in figure 2.

distribution designated as Cl–F does not deviate much from symmetric. The distributions of polyhedrons constructed for different types of halogen ions by the number of faces are shown in figure 6. The locations of the maxima of these distributions fall in values from $n^* = 10$ (F–Cl) to $n^* = 14$ (F–I).

The distribution of polyhedron faces by the number of sides reflects the rotational symmetry of the system under consideration (figure 7). As seen from figure 5, the maxima m of the distributions of all the studied systems of halogens fall at the value $m^* = 5$. This means that each of the systems under consideration has a rotational symmetry of the fifth order characteristic of a liquid [41]. The closest to a fluid with rotational symmetry of the fifth order is the F–Cl system, for which the most probable location of the maximum m of the distribution falls on $m_{\text{m.p.}} = 5.17$, and the F–I system has the strongest deviation, for which $m_{\text{m.p.}} = 5.63$. For the F–Cl system, the minimum number (432) of potential geometric neighbors is considered with a relatively small number (864) of the constructed polyhedra. In the F–I system, the number of potential neighbors selected from halogens is maximum (3200).

All the obtained distributions of the elements of the combined polyhedra are of the same type, which indicates the absence of associates in the investigated salt melt. Standard deviations for the distributions of polyhedra and their faces shown in figures 6 and 7 are present in figure 8. It can be seen that the minimum values of standard deviations correspond to polyhedra specified as F–I and Cl–I. The broadening of n spectra and partly m spectra, which leads to an increase in the

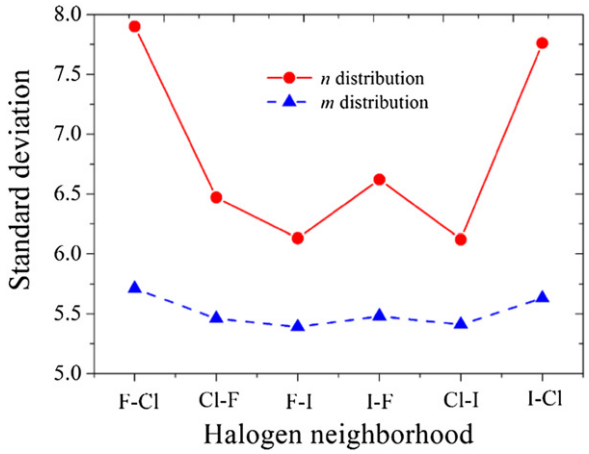

Figure 8. Standard deviations for the n- and m-distributions of neighboring halogen ions in the KF–KCl–KI salt melt at 1000 K.

corresponding standard deviations, can occur due to the formation of polyhedra with a large number of faces and faces with a large number of sides. In a condensed system, an increase in the number of geometric elements in polyhedrons occurs either due to the intensification of thermal motion, or due to a large difference in the sizes of ions. The appearance of small faces and sides in faces is the geometric manifestation of this in both cases [42, 43].

The distributions of the distances to the nearest geometric neighbors (L_n distributions) in the KF–KCl–KI melt are shown in figure 9. In a condensed system, large distances to the nearest geometric neighbors cause the appearance of

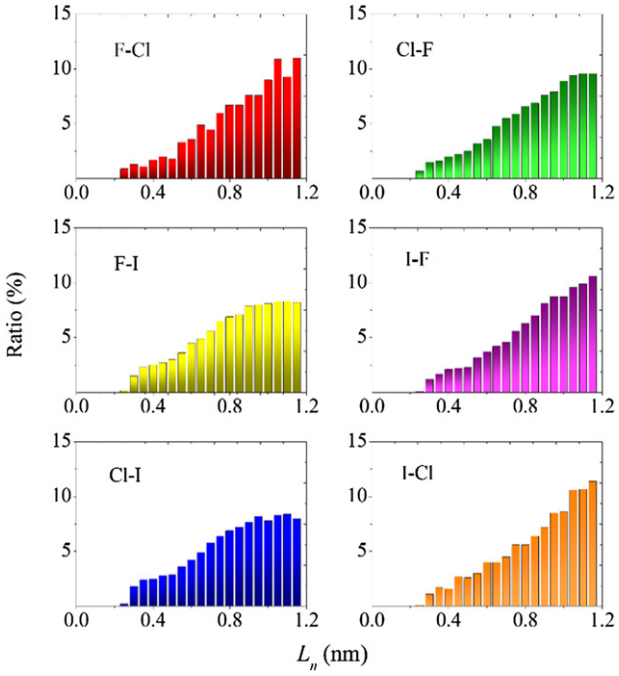

Figure 9. The ratio between the numbers of possible distances to the nearest geometric neighbors in the KF–KCl–KI salt melt at a temperature of 1000 K; the symbols of chemical elements in the field of each figure have the same meaning as the symbols in figure 2.

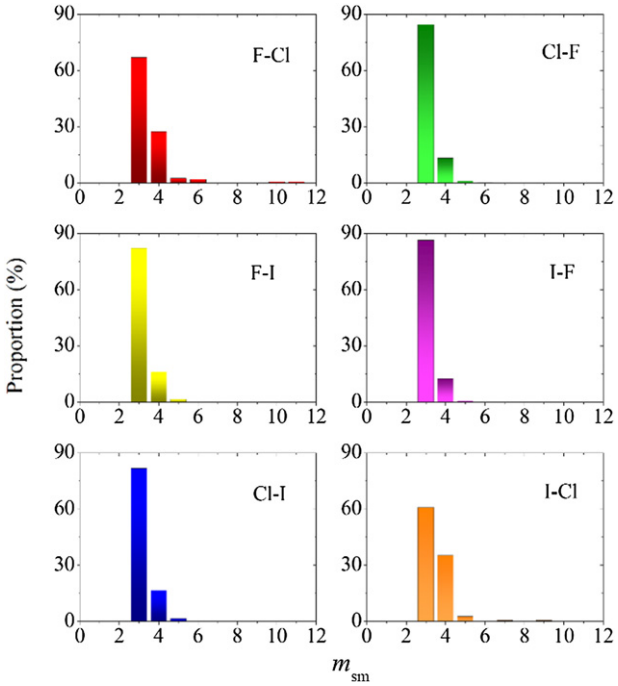

Figure 10. The proportion between the numbers of small VP faces established at a time interval of 20 ns in a statistical structural analysis of the salt melt KF–KCl–KI at a temperature of 1000 K.

small faces in the corresponding VP or combined polyhedra. When the number of ions, which are considered as possible neighbors, significantly exceeds the number of ions around which polyhedrons are built, the growth of the number of significantly distant neighbors stops. This situation is observed, for example, for polyhedra indexed as F–I and Cl–I, as well as in a weakly expressed form for polyhedra defined as Cl–F. All the distributions shown in figure 9 show the quantitative superiority of small faces over large ones, formed mainly by direct neighbors [44]. This is due to the significant difference in the sizes of the ions involved in the construction of polyhedrons, and the difference in the mobility of these ions. The ions in the considered melt have the following size ratio: $R_I/R_F = 1.65$, $R_I/R_{Cl} = 1.21$, and $R_{Cl}/R_F = 1.36$. Ratios of the ion diffusion coefficients calculated by us are as follows: $D_I/D_F = 0.59$, $D_I/D_{Cl} = 0.92$, and $D_{Cl}/D_F = 0.63$.

Simplified polyhedra were constructed by including only direct neighbors [45]. Comparison of the composition of the faces of complete (exact) and simplified polyhedra allows us to identify small faces, the composition of which for the systems under study is shown in figure 10. As a rule, the distributions of small faces in the number of sides (m_{sm}) obtained in this way are close to the corresponding distributions constructed by finding small edges (and, therefore, small faces) with length $l \leqslant 0.5\langle l\rangle$ in polyhedrons, where $\langle l\rangle$ is the average length of an edge of a polyhedron [46]. The application of the procedure for eliminating small geometric elements in polyhedra brings n and m distributions closer to the results obtained by averaging over time. In other words, the use of such a procedure makes it possible to sufficiently exclude the influence of 'thermal noise' produced by small-scale vibrations of atoms on the statistical structural characteristics.

As seen from figure 10 the vast majority (61% to 86%) of the small faces are triangular. A fairly high proportion of quadrangular small faces is found only in cases where the neighbors for species F and I are sampled from Cl^- ions: 27% and 35%, respectively. This is due to the low concentration of Cl^- ions in the melt. The distributions of simplified combined polyhedra by the number of faces and their faces by the number of sides are shown in figures S1–S6 in supplementary material (https://stacks.iop.org/JPCM/33/495103/mmedia).

Figure 11 shows the frequencies of occurrence of single and multiple bonds between different ions and demonstrates a high degree of mixing of ions in the salt melt. In the designation of ion pairs in the figure, the first symbol indicates the ion for which bonds with the ion indicated by the second symbol are considered. Near each bar shown in the figure, the calculated length of the corresponding bond between the ions is given. As can be seen from the figure, in all cases, for halogen ions of different types, single bonds dominate, the number of which can reach 96% (F–Cl). The largest number of double (14.9%) and triple (1.3%) bonds among them is established for the least represented ions (Cl^-), when the most numerous ions (I^-) are in their immediate vicinity. In the case of double contacts between ions, the bond length between them, as a rule, slightly (up to 1%) increases with respect to the single neighborhood. However, when the least represented and most numerous among halogen ions are in contact, i.e. Cl^- and I^- ions, the ratio between these types of bonds becomes opposite. Similar characteristics for ions of the same type are shown in figure S7.

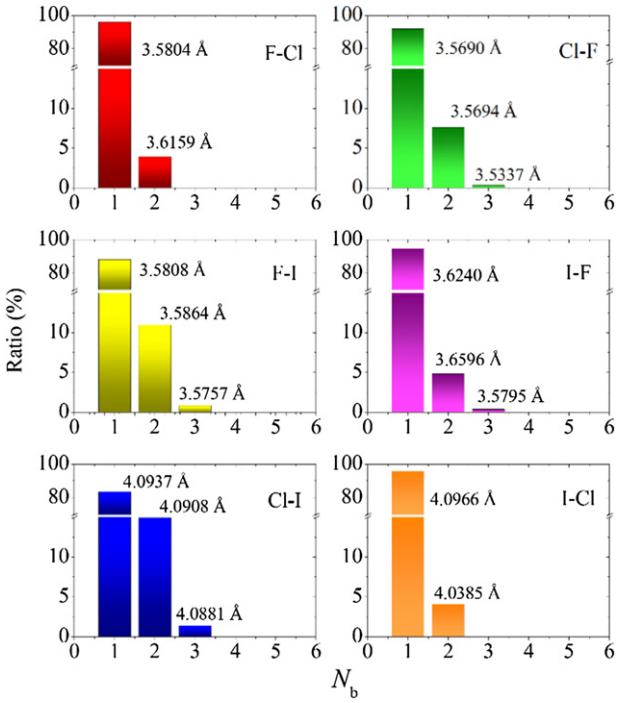

Figure 11. The ratio of the multiplicity of bonds between ionic pairs in the salt melt KF–KCl–KI at $T = 1000$ K; the corresponding bond lengths are also indicated.

The presence of dense groups of particles in an ionic liquid is explained by the following circumstances. Structural relaxation in a liquid medium is uneven. Due to the presence of short-range order in the structure of the liquid, it becomes possible to create and short-term retention of local stresses [47]. External disturbance affects the local areas of tension and local areas of compression in different ways. Relaxation in stretched areas is much faster than in compressed areas. Therefore, as a rule, structural relaxation in a liquid is not described by one character time. Local packings of atoms of different sizes are denser and express greater elasticity than that from atoms of the same size. The number of close contacts increases when the heaviest of the ions in question are grouped around the selected ion.

3. Conclusion

In a molecular dynamics model, a KF–KCl–KI salt melt was investigated at a temperature of 1000 K. The detailed structure of this melt was studied by the method of statistical geometry, based on the construction of combined polyhedra of the Voronoi polyhedron type. The identity of the partial radial distribution functions is shown, differing only in the permutation of their defining indices. The dependence of the location of the peaks of these functions on the size of the ions determining them is revealed. It is shown that the angular distributions of the nearest geometric neighbors have a dome-like shape, which is characteristic of a multicomponent liquid with components differing in atomic size. The presence of a heavy component in the melt (in this case, iodine) reduces the 'thermal noise', which is expressed as an increase in the standard deviation for the statistical distributions of the elements of the combined polyhedra. All the studied halogen subsystems are most likely characterized by rotational symmetry of the fifth order, which serves as a distinctive feature of the liquid state. The distributions of distances to the nearest geometric neighbors decrease their intensity in the region of large distances at a high concentration of desired neighbors. The small faces of the combined polyhedra, which determine the 'thermal noise' in the molten salt, are predominantly triangular in shape. However, when the number of geometric neighbors (such as Cl) is not large enough, the contribution of small quadrangular faces becomes noticeable. It was found that halogens of two different types in the investigated salt melt can have from one to three close contacts, which create short-term dynamic bonds. However, single contacts of halogen ions of different types are predominant and in all cases account for more than 83%.

The results of calculating the salt melt at a temperature of 1000 K showed that at this temperature the Born–Mayer potential has insufficient rigidity in describing short-range interactions not only between cations and anions, but also between ions with the same charges. This leads to the possibility of the presence of strong bringing ions closer together (with up to 30% smaller mutual distances) in the system than it is allowed in the presence of absolute hardness ions. This problem may be the subject of future research.

Thus, the study of the KF–KCl–KI salt melt showed a fairly uniform distribution of halogens over its volume and the absence of a tendency toward the formation of associates in it. In this case, the melt had a composition and temperature close to the corresponding characteristics of the electrolyte used to obtain solar silicon.

Acknowledgments

This work was carried out in the framework of Agreement No. 075-03-2020-582/1 of 02/18/2020 (Topic Number 0836-2020-0037).

Notes

The authors declare no competing financial interests.

Data availability statement

All data that support the findings of this study are included within the article (and any supplementary files).

ORCID iDs

Alexander Y Galashev https://orcid.org/0000-0002-2705-1946

References

[1] Ribeyron P-J 2017 Crystalline silicon solar cells: better than ever *Nat. Energy* **2** 17067

[2] Lewis N S 2016 Research opportunities to advance solar energy utilization *Science* **351** aad1920

[3] Yasuda K, Maeda K, Nohira T, Hagiwara R and Homma T 2016 Silicon electrodeposition in water-soluble KF–KCl molten salt: optimization of electrolysis conditions at 923 K *J. Electrochem. Soc.* **163** 95D–9

[4] Gu J, Fahrenkrug E and Maldonado S 2013 Direct electrodeposition of crystalline silicon at low temperatures *J. Am. Chem. Soc.* **135** 1684–7

[5] Xiao W and Wang D 2014 The electrochemical reduction processes of solid compounds in high temperature molten salts *Chem. Soc. Rev.* **43** 3215–28

[6] Link S, Ivanov S, Dimitrova A, Krischok S and Bund A 2019 Electrochemical deposition of silicon from a sulfolane-based electrolyte: effect of applied potential *Electrochem. Commun.* **103** 7–11

[7] Zaykov Y P, Zhuk S I, Isakov A V, Grishenkova O V and Isaev V A 2015 Electrochemical nucleation and growth of silicon in the KF–KCl–K 2SiF6 melt *J. Solid State Electrochem.* **19** 1341–5

[8] Bieber A L, Massot L, Gibilaro M, Cassayre L, Taxil P and Chamelot P 2012 Silicon electrodeposition in molten fluorides *Electrochim. Acta* **62** 282–9

[9] Zhao G, Meng Y, Zhang N and Sun K 2012 Electrodeposited Si film with excellent stability and high rate performance for lithium-ion battery anodes *Mater. Lett.* **76** 55–8

[10] Vlaic C A, Ivanov S, Peipmann R, Eisenhardt A, Himmerlich M, Krischok S and Bund A 2015 Electrochemical lithiation of thin silicon based layers potentiostatically deposited from ionic liquid *Electrochim. Acta* **168** 403–13

[11] Laptev M V, Isakov A V, Grishenkova O V, Vorob'ev A S, Khudorozhkova A O, Akashev L A and Zaikov Y P 2020 Electrodeposition of thin silicon films from the KF–KCl–KI–K 2SiF6 melt *J. Electrochem. Soc.* **167** 042506

[12] Khudorozhkova A O, Isakov A V, Red'kin A A and Zaikov Y P 2019 Liquidus temperatures of KF–KCl–KI melts *Russ. Metall.* **2019** 830–4

[13] Ivanichkina K A, Galashev A Y and Isakov A V 2021 Computational modeling of electrolytic deposition of a single-layer silicon film on silver and graphite substrates *Appl. Surf. Sci.* **561** 149959

[14] Born M and Mayer J E 1932 Zur gittertheorie der ionenkristalle *Z. Phys.* **75** 1–18

[15] Mayer J E 1933 Dispersion and polarizability and the van der Waals potential in the alkali halides *J. Chem. Phys.* **1** 270–9

[16] Huggins M L and Mayer J E 1933 Interatomic distances in crystals of the alkali halides *J. Chem. Phys.* **1** 643–6

[17] Huggins M L 1937 Lattice energies, equilibrium distances, compressibilities and characteristic frequencies of alkali halide crystals *J. Chem. Phys.* **5** 143–8

[18] Fumi F G and Tosi M P 1964 Ionic sizes and born repulsive parameters in the NaCl-type alkali halides-I *J. Phys. Chem. Solids* **25** 31–43

[19] Wilson M and Madden P A 1993 Polarization effects in ionic systems from first principles *J. Phys.: Condens. Matter.* **5** 2687–706

[20] Aragones J L, Sanz E, Valeriani C and Vega C 2012 Calculation of the melting point of alkali halides by means of computer simulations *J. Chem. Phys.* **137** 104507

[21] Smith D E and Dang L X 1994 Computer simulations of NaCl association in polarizable water *J. Chem. Phys.* **100** 3757–66

[22] Joung I and Cheatham T 2008 Determination of alkali and halide monovalent ion parameters for use in explicitly solvated biomolecular simulations *J. Phys. Chem* B **112** 9020–9041

[23] Wu J, Wang J, Ni H, Lu G and Yu J 2018 The influence of NaCl concentration on the (LiCl–KCl) eutectic system and temperature dependence of the ternary system *J. Mol. Liq.* **253** 96–112

[24] Matsumiya M, Shin W, Izu N and Murayama N 2002 Investigation on the electrical properties of molten quaternary systems (Li, Na, K, Cs)Cl and (Li, Na, K, Cs)F by MD simulation *J. Electroanal. Chem.* **528** 103–13

[25] Wu J, Wang J, Ni H, Lu G and Yu J 2018 Investigation of microscopic structure and ion dynamics in liquid Li(Na, K) Eutectic Cl systems by molecular dynamics simulation *Appl. Sci.* **8** 1874

[26] Wang Y, Shao J and Zhu X 2012 The melting and freezing of KI nanoparticles confined within zigzag single-walled carbon nanotubes based on molecular dynamics simulations *Comput. Theor. Chem.* **983** 38–44

[27] Laudernet Y, Cartailler T, Turq P and Ferrario M 2003 A microscopic description of concentrated potassium fluoride aqueous solutions by molecular dynamics simulation *J. Phys. Chem* B **107** 2354–61

[28] Zakiryanov D 2021 Non-empirical calculations of melting temperatures, thermal conductivity coefficients and local structure of halogenide and oxyhalogenide melts *Dissertation for a Scientific Degree Candidate of Chemical sciences* Yekaterinburg. Institute of High-Temperature Electrochemistry, Ural Branch of the Russian Academy of Sciences

[29] Sangster M J L and Dixon M 1976 Interionic potentials in alkali halides and their use in simulations of the molten salts *Adv. Phys.* **25** 247–342

[30] Baranyai A 2020 Alkali halide force fields: a search for an acceptable compromise *J. Mol. Liq.* **297** 111762

[31] Ji S 2004 A generalized mixture rule for estimating the viscosity of solid–liquid suspensions and mechanical properties of polyphase rocks and composite materials *J. Geophys. Res.* **109** B10207

[32] Khudorozhkova A O, Isakov A V, Kataev A A, Red'kin A A and Zaikov Y P 2020 Density of KF–KCl–KI melts *Russ. Metall.* **2020** 918–24

[33] Pan G-C, Ding J, Wang W, Lu J, Li J and Wei X 2016 Molecular simulations of the thermal and transport properties of alkali chloride salts for high-temperature thermal energy storage *Int. J. Heat Mass Transfer* **103** 417–27

[34] Frandsen B A, Nickerson S D, Clark A D, Solano A, Baral R, Williams J, Neuefeind J and Memmott M 2020 The structure of molten FLiNaK *J. Nucl. Mater.* **537** 152219

[35] Tersoff J 1989 Modeling solid-state chemistry: interatomic potentials for multicomponent systems *Phys. Rev.* B **39** 5566–8

[36] Galashev A Y and Ivanichkina K A 2019 Computational investigation of a promising Si–Cu anode material *Phys. Chem. Chem. Phys.* **21** 12310–20

[37] Galashev A E 1996 Vitrification and structural differences between metal glass, quasicrystal, and Frank–Kasper phases *J. Struct. Chem.* **37** 120–36

[38] Galashev A E and Skripov V P 1984 Investigation on the disordering of argon hexagonal closed packed (HCP) crystals by the method of statistical geometry *J. Struct. Chem.* **25** 734–40

[39] Galashev A E 2010 Computer investigation of the structure of a porous SiO_2 nanoparticle under uniform tension *Glass Phys. Chem.* **36** 589–97

[40] Galashev A E and Skripov V P 1986 Stability and structure of a two-component crystal using a molecular dynamics model *J. Struct. Chem.* **27** 407–12
[41] Galashev A E 2014 Structure of water clusters with captured methane molecules *Russ. J. Phys. Chem.* B **8** 793–800
[42] Galashev A E 2013 Computer study of the spectral characteristics and structures of (GaN)54(SiO2)50 nanoparticles *J. Synch. Invest.* **7** 788–96
[43] Novruzova O A, Rakhmanova O P and Galashev A E 2007 The stability and structure of (N2)*j*(H2O)*i* and (Ar)*j*(H2O)*i* clusters *Russ. J. Phys. Chem.* **81** 1825–8
[44] Brostow W, Dussault J-P and Fox B L 1978 Construction of Voronoi polyhedra *J. Comput. Phys.* **29** 81–92
[45] Galashev A Y 2020 Computational investigation of silicene/nickel anode for lithium-ion battery *Solid State Ionics* **357** 115463
[46] Galashev A Y, Ivanichkina K A and Zaikov Y P 2020 Computational study of physical properties of low oxygen UO_{2-x} compounds *J. Solid State Chem.* **286** 121278
[47] Trachenko K K and Zaccone A 2021 Slow stretched-exponential and fast compressed-exponential relaxation from local event dynamics *J. Phys.: Condens. Matter.* **33** 315101